International Journal of Solids and Structures 193–194 (2020) 393–404

Contents lists available at ScienceDirect

International Journal of Solids and Structures

journal homepage: www.elsevier.com/locate/ijsolstr

Visco-hyperelastic material modeling using nested linkage mechanisms

M Umut Ozcan, Cetin Yilmaz*, Fazil O. Sonmez

Department of Mechanical Engineering, Bogazici University, Istanbul, Bebek 34342, Turkey

ARTICLE INFO

Article history:
Received 19 September 2019
Revised 19 February 2020
Accepted 24 February 2020
Available online 26 February 2020

Keywords:
Viscoelasticity
Hyperelasticity
Hysteresis
Dynamic stiffness
Mechanisms
Linear lumped elements

ABSTRACT

In this study, basic linear lumped elements such as springs and dashpots are used in nested linkage mechanisms in order to simulate the mechanical behavior of visco-hyperelastic materials. The proposed mechanism model containing two nested linkages can show initial softening followed by hardening response under quasi-static loading, which is commonly displayed by hyperelastic materials. Hence, material nonlinearity is simulated by geometric nonlinearity of the linkage mechanism. The mechanism also displays relaxation, hysteresis, and dynamic stiffness responses of viscoelastic materials with the help of dashpot elements. Visco-hyperelastic material behavior is closely approximated by the proposed mechanism model for the four different test scenarios, i.e., quasi-static loading, ramp-and-hold loading, hysteresis, and dynamic stiffness tests. It is shown that nonlinearity and frequency dependency of visco-hyperelastic materials is successfully captured.

1. Introduction

Visco-hyperelastic materials are widely used in various industrial areas from automotive to medical applications. Passive vibration isolators and absorbers, and most of the damping systems are made of elastomers, rubbers, or other visco-hyperelastic materials. In surgical training organs, and in some other medical applications, visco-hyperelastic materials are used. As these materials possess both viscoelastic and hyperelastic features, their response under different loading conditions is complex. In order to fully describe the structural response of the material, different loading scenarios need to be considered. The material exhibits nonlinear stress-strain response under quasi-static loading; typically it first softens, and then stiffens with increased strain. The material shows hysteresis response when subjected to loading and unloading cycles. Relaxation response is elicited with a ramp-and-hold loading. Dynamic (frequency-dependent) stiffness response is obtained by cyclic loading at varying frequencies. These four main characteristics of visco-hyperelastic materials need to be considered to model their mechanical behavior in typical applications.

Visco-hyperelastic materials exhibit different stiffness responses during loading and unloading. Because the stress-strain curves during loading and unloading are different, thus, the area under the curve is different. The material absorbs energy in each load cycle, which is called “hysteresis”. Damping of vibrations in viscoelastic material systems occurs due to hysteresis. Many researchers (Abe et al., 2004; Agoras et al., 2009; Bergstrom and Boyce, 1998; Buhan et al., 2015; Khajehsaeid et al., 2013; Mansouri and Darijani, 2014; Rey et al., 2014; Vieira et al., 2014) studied hyperelastic structural response as well as hysteresis behavior of visco-hyperelastic materials under quasi-static loading. Constitutive equations and analytical formulations were developed to describe nonlinear hyperelastic response. In these studies, material nonlinearities were accounted for by defining nonlinear material properties in constitutive models or using nonlinear elements in rheological models like nonlinear springs and dashpots.

Stress relaxation response of viscoelastic materials under ramp-and-hold loading was also extensively studied in the literature (Bergstrom and Boyce, 2000; Bhuiyan et al., 2009; Drozdov, 1997; Feng and Gan, 2002; Muliana et al., 2016; Pellicer and Morales, 2004; Saitoh, 2012; Tam et al., 2015; Wang and Han, 2013). In this loading scenario, following a quickly applied compressive strain, the specimen is kept at constant strain. The magnitude of the stress drops with a decreasing rate and reaches a steady value in the long run. Relaxation behavior varies with material type, sample geometry, loading rate, applied strain, temperature, humidity, and composition (Wang and Han, 2013). The analytical rheological models and the numerical models based on linear springs and dashpots can mimic relaxation response

* Corresponding author.
E-mail address: cetin.yilmaz@boun.edu.tr (C. Yilmaz).

https://doi.org/10.1016/j.ijsolstr.2020.02.035
0020-7683/

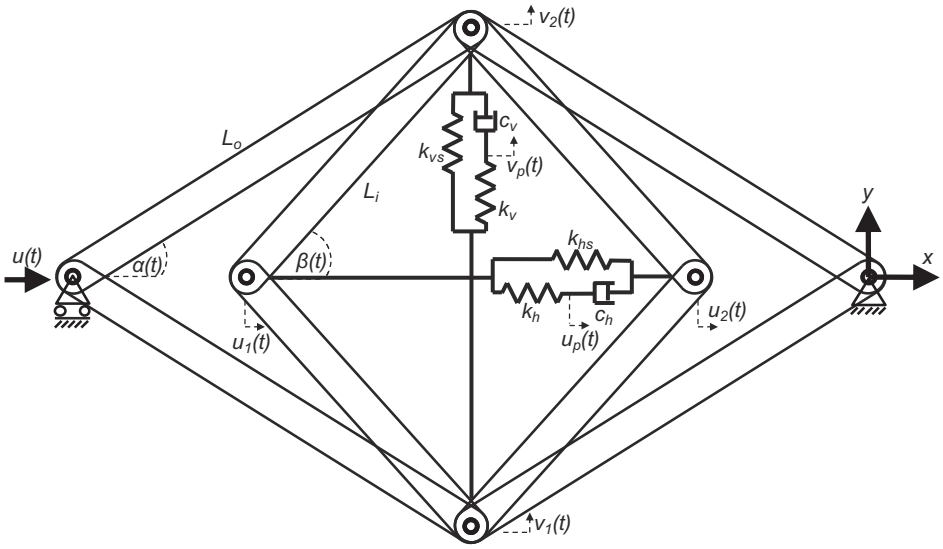

Fig. 1. The proposed mechanism model that mimics the mechanical behavior of visco-hyperelastic materials.

as well as dynamic stiffness response, but not nonlinear hyperelastic response. Only by using nonlinear springs and dashpots, a few models (Bergstrom and Boyce, 2000; Bhuiyan et al. 2009; Drozdov, 1997; Tam, 2015) account for visco-hyperelastic material response in both quasi-static and ramp-and-hold test scenarios.

Visco-hyperelastic materials under dynamic loading exhibit increasing stiffness response with an increase in frequency due to material damping. Dynamic stiffness response of visco-hyperelastic materials was investigated usually via constitutive models or rheological models using linear elements. (Carleo et al., 2017; Iniguez-Macedo et al., 2019; Renaud et al., 2011; Wollscheid and Lion, 2013; Zoffoli et al., 2017) In some studies (Bhuiyan et al., 2009; Lewandowski and Chorazyczewski, 2010; Osterlof et al., 2014; Xu et al., 2018) complex elements such as frequency dependent springs and dashpots are used to capture the dynamic response more closely.

Some researchers developed analytical models for material responses under two different loading conditions such as quasi-static response and creep recovery (Muliana et al., 2016), relaxation and hysteresis response (Bergstrom and Boyce, 1998; Drozdov, 1997; Vandenbroucke et al., 2010), hysteresis and dynamic-stiffness response (Rendek and Lion, 2010) and quasi-static, relaxation, and dynamic-stiffness responses (Kamaruddin et al., 2017). In some studies (Acar and Yilmaz, 2013; Hegde and Ananthasuresh, 2012; Kim et al., 2014; Yilmaz et al., 2007; Yilmaz and Hulbert, 2010; Yuksel and Yilmaz, 2015), responses of various structures were investigated by using linkage mechanisms to model their frequency-dependent response or structural response, but these studies did not focus on visco-hyperelastic materials. In some other studies (Holecek and Moravec, 2006; Natsupakpong and Cavusoglu, 2010; Noborio and Oohara, 2009; San-Vicente et al., 2012), material models were developed with lattice structures composed of linear lumped elements. As the lattice deforms, orientations of the linear elements significantly change with respect to each other because of the geometry. Hence, nonlinear material response can be simulated by the geometric nonlinearity of the lattice structure. These studies considered only a single test scenario such as quasi-static tension or compression.

In this study, a mechanism-based model is developed using a small number of parameters to represent the complex mechanical behavior of visco-hyperelastic materials. In the proposed model, the mechanism contains only rigid links and linear lumped elements, i.e., springs and dashpots. Material nonlinearity is simulated by geometric nonlinearity of the linkage mechanism, while in the previous models this is mostly achieved by defining nonlinear material properties or using nonlinear spring or dashpot elements. In the literature, different models were proposed for different loading conditions to simulate the response of visco-hyperelastic materials. For instance, the commonly used Maxwell, Generalized Maxwell, Kelvin-Voigt, Standard Linear Solid and Burgers models are capable of displaying relaxation response and/or dynamic stiffness response, but they cannot show nonlinear softening-hardening behavior in quasi-static loading. In contrast, the mechanism-based model proposed in this study can mimic the nonlinear force-displacement, stress relaxation, hysteresis, and dynamic stiffness characteristics of visco-hyperelastic materials with the same parameter values. As far as the authors know, there is no mechanical model in the literature that can mimic the response of visco-hyperelastic materials under these four loading scenarios.

2. The mechanism model

The mechanism model that will be used to mimic the mechanical behavior of visco-hyperelastic materials includes two nested parallelogram linkages as shown in Fig. 1. The inner and outer loops are connected by two pin joints. The opposite joints of the inner loop are connected by springs having stiffness k_{hs} and k_{vs}. Additionally, parallel to these springs (k_{hs} and k_{vs}), serially connected springs and dashpots are used with stiffness and damping coefficients k_h, c_h and k_v, c_v respectively. k_{hs}, k_h and c_h form a standard linear solid (SLS) model arm in horizontal direction, whereas k_{vs}, k_v and c_v form another one in vertical direction. These two SLS model arms are displaced at different rates due to the nonlinear geometry of the mechanism. The movement of the right-most joint is restrained and load is applied to the left-most joint along the x-direction. The inner mechanism loop has shorter links ($L_i < L_o$). Consequently, $\beta(t)$ is always greater than $\alpha(t)$ for any value of the input displacement $u(t)$. Moreover, the mechanism has one degree of freedom. Given the displacement of the left joint ($u(t)$) and the initial configuration of the mechanism, its mechanical response can be completely determined.

Dynamic analysis of the proposed model is performed analytically. Horizontal displacement (u) of the left side of the nested mechanism is the only generalized coordinate of this single-degree-of-freedom mechanism. The vertical displacements v_1 and v_2, the horizontal displacements u_1 and u_2 and the angles α and β

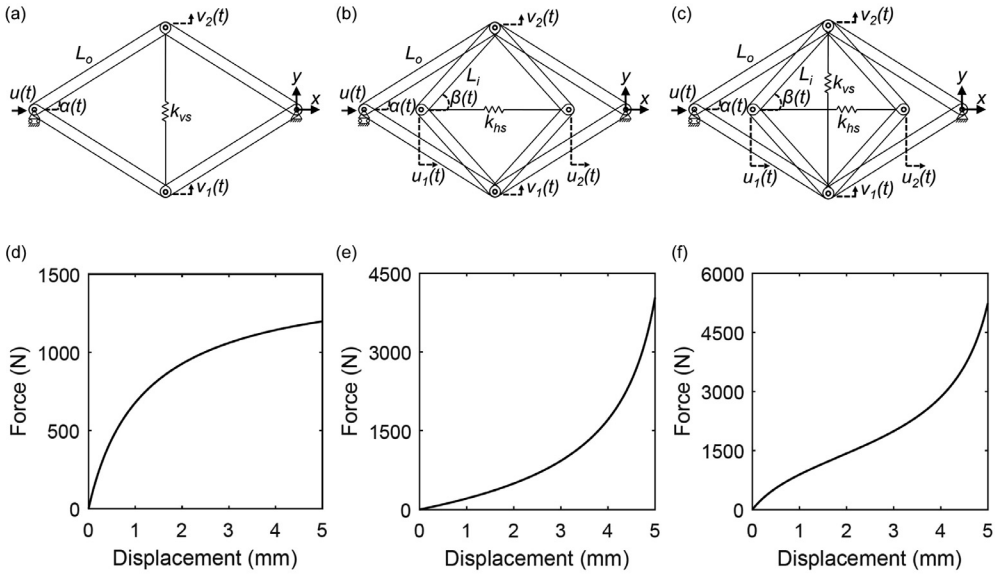

Fig. 2. (a) Vertical spring and outer four-bar linkage, (b) horizontal spring, inner and outer four-bar linkages, (c) Horizontal and vertical springs, inner and outer four-bar linkages. (d) Effect of vertical spring as softening response, (e) effect of horizontal spring as hardening response, (f) combined effect of horizontal and vertical springs as initial softening and later hardening response. Response is obtained for 10 mm compression with parameter values given in Table 1.

Table 1
The reference configuration for the proposed model.

k_{hs} (N/mm)	k_h (N/mm)	c_h (Ns/mm)	k_{vs} (N/mm)	k_{vs} (N/mm)	c_v (Ns/mm)	L_o (mm)	L_i (mm)	α (deg)
10	10	10	10	10	10	100	35	7

can be obtained in terms of u. Auxiliary points are added between k_h and c_h, and k_v and c_v with displacements u_p and v_p, respectively as shown in Fig. 1. Hence, there are two more degrees of freedom of this system when the coupling points are considered.

First, the relations between the geometric parameters are derived. The current length of the mechanism is equal to the distance between the left most joint and the origin. The horizontal length of the system is ℓ and its initial value is ℓ_i. The angle of the outer links, α, is related to u and the length of the outer links, L_o, as

$$\ell = \ell_i - u = 2L_o \cos\alpha \tag{1}$$

As the input displacement (u) increases, the length of the mechanism decreases with a rate given by

$$\frac{d\ell}{dt} = -\frac{du}{dt} \tag{2}$$

Solving for α in Eq. (1), one obtains

$$\alpha = \cos^{-1}\left(\frac{\ell}{2L_o}\right) \tag{3}$$

β should be larger than α and it can determined by the following equation

$$sin\beta = \frac{L_o}{L_i} sin\alpha \tag{4}$$

Substituting α in Eq. (3) into Eq. (4) and using the following relation

$$\sin\left(\cos^{-1}\varphi\right) = \sqrt{1-\varphi^2} \tag{5}$$

β can be expressed as

$$\beta = sin^{-1}\left(\frac{L_o}{L_i}\sqrt{1-\left(\frac{\ell}{2L_o}\right)^2}\right) \tag{6}$$

The positions of the inner link joints, x_1, x_2, their displacements u_1, u_2, and their first time derivatives are calculated as follows

$$x_1 = -L_o cos(\alpha) - L_i cos(\beta) \tag{7}$$

Substituting Eq. (3) and Eq. (6) into Eq. (7) and making use of Eq. (5), Eq. (7) becomes

$$x_1 = -\frac{1}{2}\left(\ell + \sqrt{\ell^2 - 4{L_o}^2 + 4{L_i}^2}\right) \tag{8}$$

Then, u_1 and $\dot{u}_1$ can be calculated as

$$u_1 = x_1 - x_{1i} = -\frac{1}{2}\left(\ell + \sqrt{\ell^2 - 4{L_o}^2 + 4{L_i}^2}\right) + \frac{1}{2}\left(\ell_0 + \sqrt{{\ell_0}^2 - 4{L_o}^2 + 4{L_i}^2}\right) \tag{9}$$

$$\dot{u}_1 = -\frac{\dot{\ell}}{2} - \frac{1}{2}\frac{\ell\,\dot{\ell}}{\sqrt{\ell^2 - 4{L_o}^2 + 4{L_i}^2}} \tag{10}$$

Similarly, x_2, u_2 and $\dot{u}_2$ are derived as

$$x_2 = -L_o cos(\alpha) + L_i cos(\beta) \tag{11}$$

$$u_2 = x_2 - x_{2i} = -\frac{1}{2}\left(\ell - \sqrt{\ell^2 - 4{L_o}^2 + 4{L_i}^2}\right) + \frac{1}{2}\left(\ell_0 - \sqrt{{\ell_0}^2 - 4{L_o}^2 + 4{L_i}^2}\right) \tag{12}$$

$$\dot{u}_2 = -\frac{\dot{\ell}}{2} + \frac{1}{2}\frac{\ell\,\dot{\ell}}{\sqrt{\ell^2 - 4{L_o}^2 + 4{L_i}^2}} \tag{13}$$

The positions of the upper and lower joints, y_1 and y_2, are given as

$$y_2 = -y_1 = L_o sin(\alpha) \tag{14}$$

Substituting Eq. (3) and making use of Eq. (5), Eq. (14) becomes

$$y_2 = -y_1 = \frac{1}{2}\sqrt{4{L_o}^2 - \ell^2} \tag{15}$$

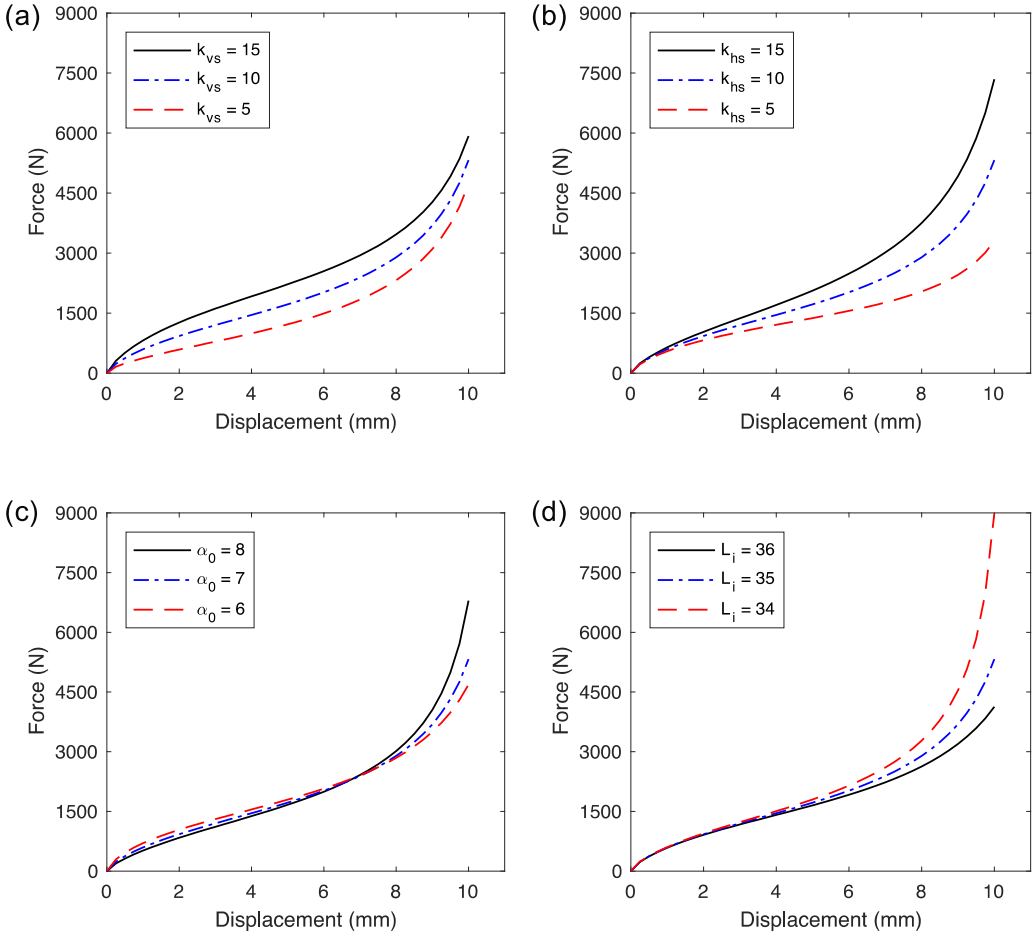

Fig. 3. The effects of (a) k_{vs}, (b) k_{hs}, (c) α_0, and (d) L_i on the response of the mechanism under quasi-static loading. The blue dashed-dotted line represents the response of the reference configuration.

Moreover, v_1, v_2, $\dot{v}_1$ and $\dot{v}_2$ are derived as

$$v_2 = -v_1 = \frac{1}{2}\sqrt{4{L_o}^2 - \ell^2} - \frac{1}{2}\sqrt{4{L_o}^2 - {\ell_0}^2} \tag{16}$$

$$\dot{v}_2 = -\dot{v}_1 = -\frac{1}{2}\frac{\ell\ \dot{\ell}}{\sqrt{4{L_o}^2 - \ell^2}} \tag{17}$$

The Maxwell arms of the inner mechanisms are composed of serially connected spring and dashpot elements (k_h and c_h; k_v and c_v). The total extension in the horizontal Maxwell arm, u_t, is given by the difference between the horizontal displacements u_1 and u_2, which is also equal to the sum of the extensions of the spring and dashpot (u_s and u_d) as

$$u_t = u_2 - u_1 = u_s + u_d \tag{18}$$

A negative value of u_t indicates contraction of the Maxwell arm. Moreover, time derivative of u_t can be obtained as

$$\dot{u}_t = \dot{u}_2 - \dot{u}_1 = \dot{u}_s + \dot{u}_d \tag{19}$$

The resistive forces of the spring and damper, F_s and F_d, due to their extension or contraction are equal to each other, since they are connected in series. For the horizontal Maxwell arm, the forces are as follows

$$F_s = F_d \text{ or } k_h u_s = c_h \dot{u}_d \tag{20}$$

Rearranging Eq. (20) gives

$$\frac{k_h}{c_h}u_s = \dot{u}_d \tag{21}$$

Substituting Eq. (21) in Eq. (19) gives

$$\dot{u}_t = \dot{u}_s + \frac{k_h}{c_h}u_s \tag{22}$$

Eq. (22) can be rewritten as

$$e^{\frac{k_h}{c_h}t}\frac{du_s}{dt} + \frac{k_h}{c_h}u_s e^{\frac{k_h}{c_h}t} = \dot{u}_t e^{\frac{k_h}{c_h}t} \tag{23}$$

Then, it can be solved as

$$\int d\left(u_s e^{\frac{k_h}{c_h}t}\right) = \int \dot{u}_t e^{\frac{k_h}{c_h}t} dt \tag{24}$$

Considering the initial condition as $u_s(0) = 0$ and taking the integral using time increments of Δt, change in the length of the spring, u_s, and its rate, $\dot{u}_s$, at time $t = i\Delta t$ is obtained as

$$u_s(\mathrm{i}\Delta\mathrm{t}) = \frac{\dot{u}_t(\mathrm{i}\Delta\mathrm{t})c_h}{k_h} - \frac{\dot{u}_t((\mathrm{i}-1)\Delta\mathrm{t})c_h}{k_h}e^{-\frac{k_h}{c_h}\Delta t} + u_s((\mathrm{i}-1)\Delta\mathrm{t})e^{-\frac{k_h}{c_h}\Delta t} \tag{25}$$

$$\dot{u}_s(\mathrm{i}\Delta\mathrm{t}) = \dot{u}_t((\mathrm{i}-1)\Delta\mathrm{t})e^{-\frac{k_h}{c_h}\Delta t} - \frac{k_h}{c_h}u_s((\mathrm{i}-1)\Delta\mathrm{t})e^{-\frac{k_h}{c_h}\Delta t} \tag{26}$$

Eqs. (25) and (26) can be explicitly calculated (for $i = 1,2, \ldots, n$) by using a predefined time step (Δt). Vertical displacement can be obtained using a similar procedure. Total force on the left side of the mechanism can easily be determined using the trigonometric relations in Eq. (27)

$$F_t(t) = (k_{hs}u_t(t) + k_h u_s(t))\tan\beta(t)\cot\alpha(t)$$

Table 2
Parameters used in Fig. 5.

	k_{hs} (N/mm)	k_h (N/mm)	c_h (Ns/mm)	k_{vs}(N/mm)	k_{vs} (N/mm)	c_v (Ns/mm)	L_o (mm)	L_i (mm)	α(deg)
Single SLS 1	10	10	3.4	–	–	–	100	35	7
Single SLS 2	10	12	0.5	–	–	–	100	35	7
Double SLS	6	10	0.15	6	7	3	100	35	7

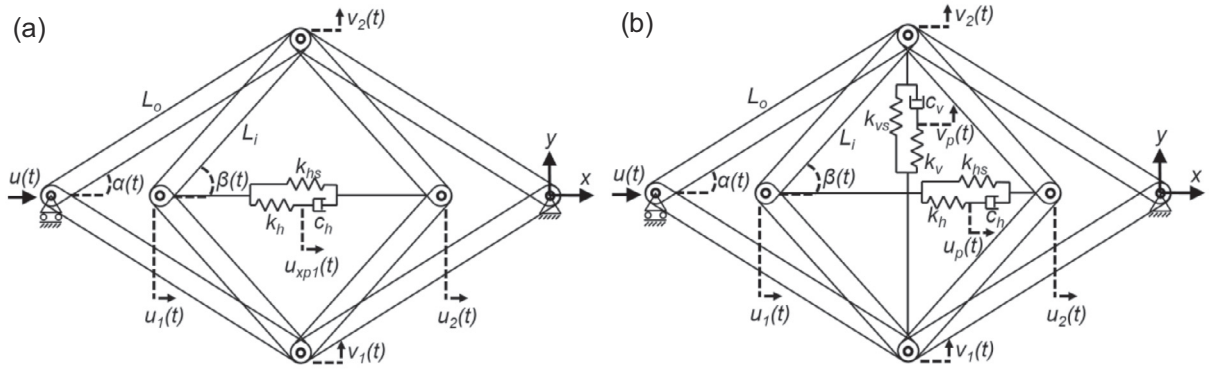

Fig. 4. (a) Single SLS element in the mechanism, (b) double SLS elements in the mechanism.

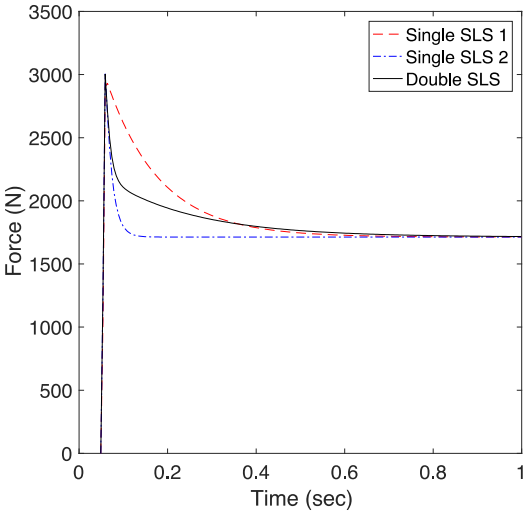

Fig. 5. The effect of different SLS configurations on relaxation response after 8 mm compression applied in 0.05 s. The parameter values are given in Table 2.

$$+w(k_{vs}v_t(t)+k_v v_s(t))\cot\alpha(t) \tag{27}$$

These calculations are conducted in MATLAB. Moreover, the same mechanism is formed in MSC ADAMS and exactly the same results are obtained for the four test scenarios (quasi-static, ramp-and-hold, hysteresis and dynamic stiffness). Hence, the MATLAB model is verified. As the MATLAB model is more time efficient, optimization studies regarding test data correlation will be conducted in MATLAB.

3. Parametric studies

The external loading is applied to the left-most joint as displacement, $u(t)$; the resistive force of the mechanism $F_t(t)$, to this movement is calculated using the analysis explained in the previous section. The mechanical response of the mechanism as force versus displacement, time, or frequency is examined for different parameter values, i.e., stiffness coefficients k_{hs}, k_{vs}, k_h and k_v, damping coefficients c_h and c_v, lengths of inner and outer links L_i and L_o and the initial angle of the outer link α_0. A parametric study is conducted in order to see how the individual parameters affect the mechanical response in four different testing scenarios and how they contribute to the simulation of visco-hyperelastic material behavior. The parameter values of the reference configuration of the system are given in Table 1. The mechanical response of the mechanism is examined by varying a single parameter and keeping the others constant.

Hyperelastic materials exhibit nonlinear mechanical response under quasi-static loading. In early phases of loading, the material shows softening behavior with increasing strain due to reorientation and alignment of polymer chains along the loading direction (Bergstrom and Boyce, 1998). This softening behavior reveals itself mostly in polymers containing reinforcing agent (carbon black) (Bergstrom and Boyce, 2000; Ren et al., 2015). At intermediate stages of loading, stiffening behavior dominates due to stretching of free polymer chains. The proposed mechanism model can exhibit this characteristic behavior. Fig. 2 shows the individual effects of a vertical spring, a horizontal spring as well as their combined effect. In this figure, k_h, k_v, c_h and c_v are not included since the force on them will be zero due to very slow loading rate. As it can be seen in Fig. 2a and d, vertical spring (k_{vs}) imparts softening behavior under quasi-static loading scenario whereas horizontal spring (k_{hs}) imparts hardening behavior (see Fig. 2b and e). A combination of vertical and horizontal springs (see Fig. 2c and f) provides an initial softening response followed by a hardening response as seen in various elastomers.

During quasi-static loading scenario, the most effective parameters are observed to be k_{vs}, k_{hs}, and α_0. As shown in Fig. 3a, the stiffness of the vertical spring k_{vs}, controls the initial softening behavior of the system. In early phases of loading, the slope of the force-displacement curve, i.e. the stiffness of the mechanism, decreases with increasing displacement. This behavior becomes more apparent with higher values of k_{vs}. The horizontal spring, on the other hand, contributes mainly to stiffening response in later stages of loading (See Fig. 3b). The initial angle of the outer links, α_0, is an effective parameter on the stiffening behavior at the later stages of the loading as seen in Fig. 3c. As it is seen in Fig. 3d, L_i mainly affects the later parts of the loading. The characteristics of the response can be adjusted by changing the values of k_{vs}, k_{hs}, α_0 and L_i. The nested links together with the horizontal spring pro-

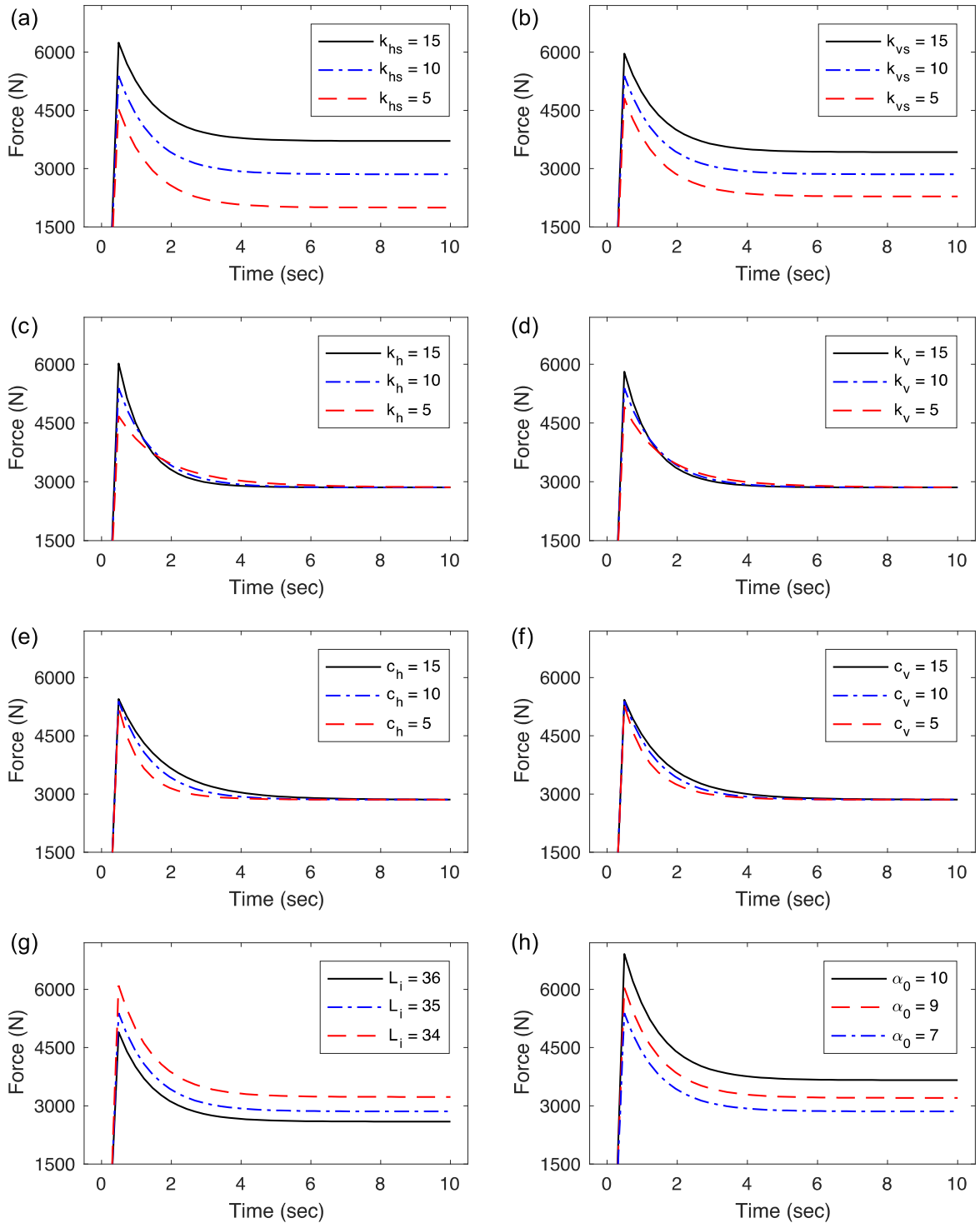

Fig. 6. The effects of (a) k_{hs}, (b) k_{vs}, (c) k_h, (d) k_v, (e) c_h, (f) c_v, (g) L_i, and (h) α_0 on the relaxation response of the mechanism under ramp-and-hold loading. The blue dashed-dotted line represents the response of the reference configuration.

vide nonlinear stiffening response because of the geometric nonlinearity of the system. The other parameters do not significantly affect the overall response in quasi-static loading.

Viscoelastic materials exhibit stress-relaxation response due to realignment of polymer chains after an applied deformation. This deformation characteristic varies mainly with the material composition, excitation velocity, and amplitude. Under ramp-and-hold loading, relaxation response is generally not uniform with a fast drop at the beginning followed by gradual relaxation. In order to simulate this characteristic behavior, the mechanism architectures in Fig. 4 are considered. Fig. 5 shows the relaxation response of different mechanism designs due to 8 mm compression applied in 0.05 s followed by one-second relaxation time. By choosing different values for the spring rate, k_h, and the damping coefficient, c_h, in the single SLS models (see Table 2), fast and slow relaxation rates are realized while the maximum force and steady state force levels remain nearly the same. The combination of horizontal and vertical SLS elements provides about the same maximum force and

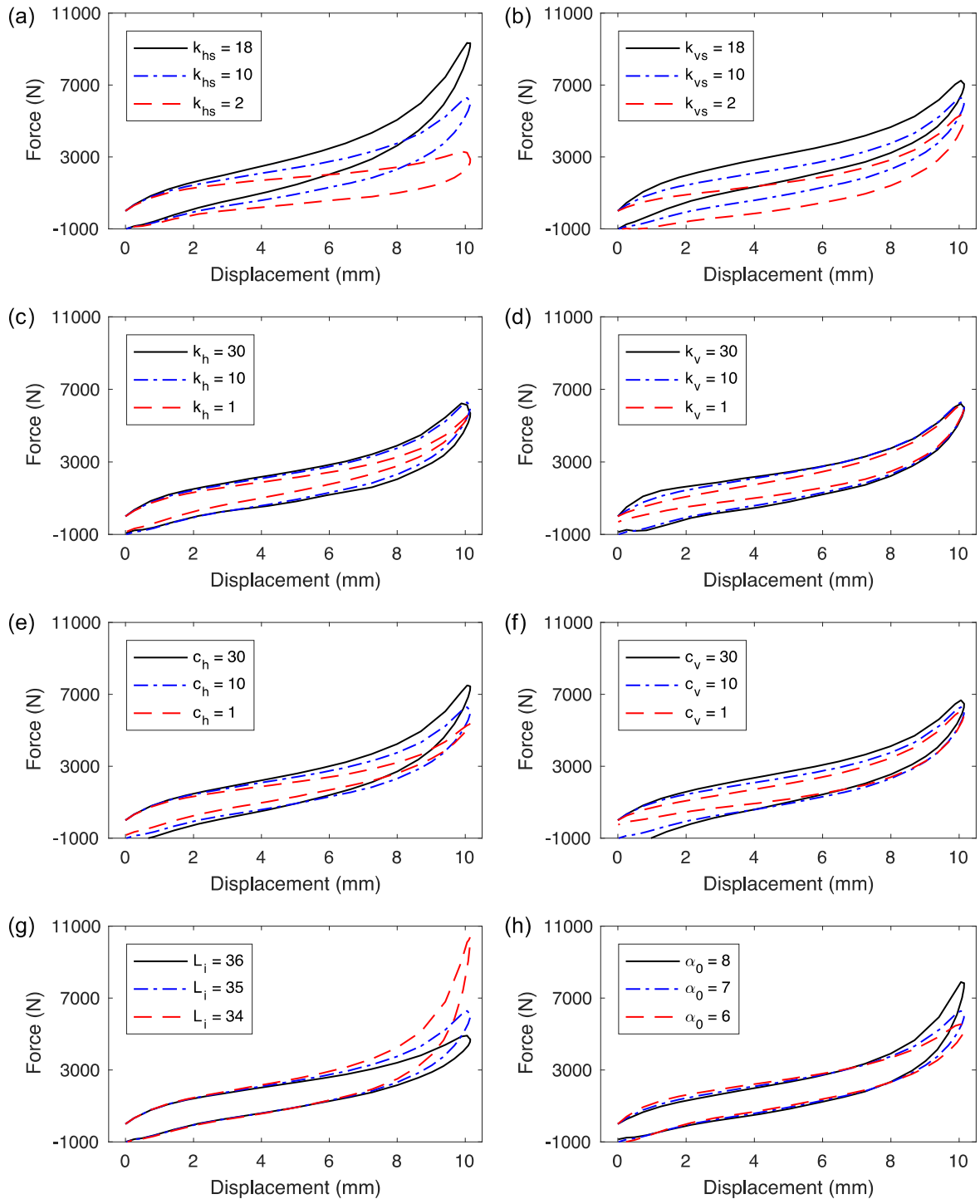

Fig. 7. The effects of (a) k_{hs}, (b) k_{vs}, (c) k_h, (d) k_v, (e) c_h, (f) c_v, (g) L_i, and (h) α_0 on the hysteresis behavior of the mechanism. The blue dashed-dotted line represents the response of the reference configuration.

the steady state force levels, but a different relaxation response. As seen in Fig. 5, the double SLS provides a similar relaxation rate as single SLS 2 in the early phases of the relaxation; but changes its characteristics such that the relaxation rate is similar to that of single SLS 1 in the later stages of relaxation. Therefore, by using double SLS, different relaxation characteristics of viscoelastic materials can be simulated that cannot be simulated by a single SLS.

Relaxation curve of viscoelastic materials is generally a complex curve that cannot be expressed with a single-term (Ciambella et al., 2010; Oman and Nagode, 2014). This is why analytical studies (Vandenbroucke et al., 2010; Wang and Han, 2013) generally use exponential formulations with minimum two terms to model relaxation response. The mechanism model proposed in this study includes two SLS elements positioned horizontally and vertically, which provide different relaxation rates due to different set of parameters (k_{hs}, k_h, c_h vs k_{vs}, k_v, c_v), and parameters for geometric nonlinearity of the mechanism (L_o, L_i, α_o). As seen in Table 1, there are nine parameters that can be changed to tune the response of the mechanism model. In order to see the effects of these parameters on the relaxation response, 8 mm displacement

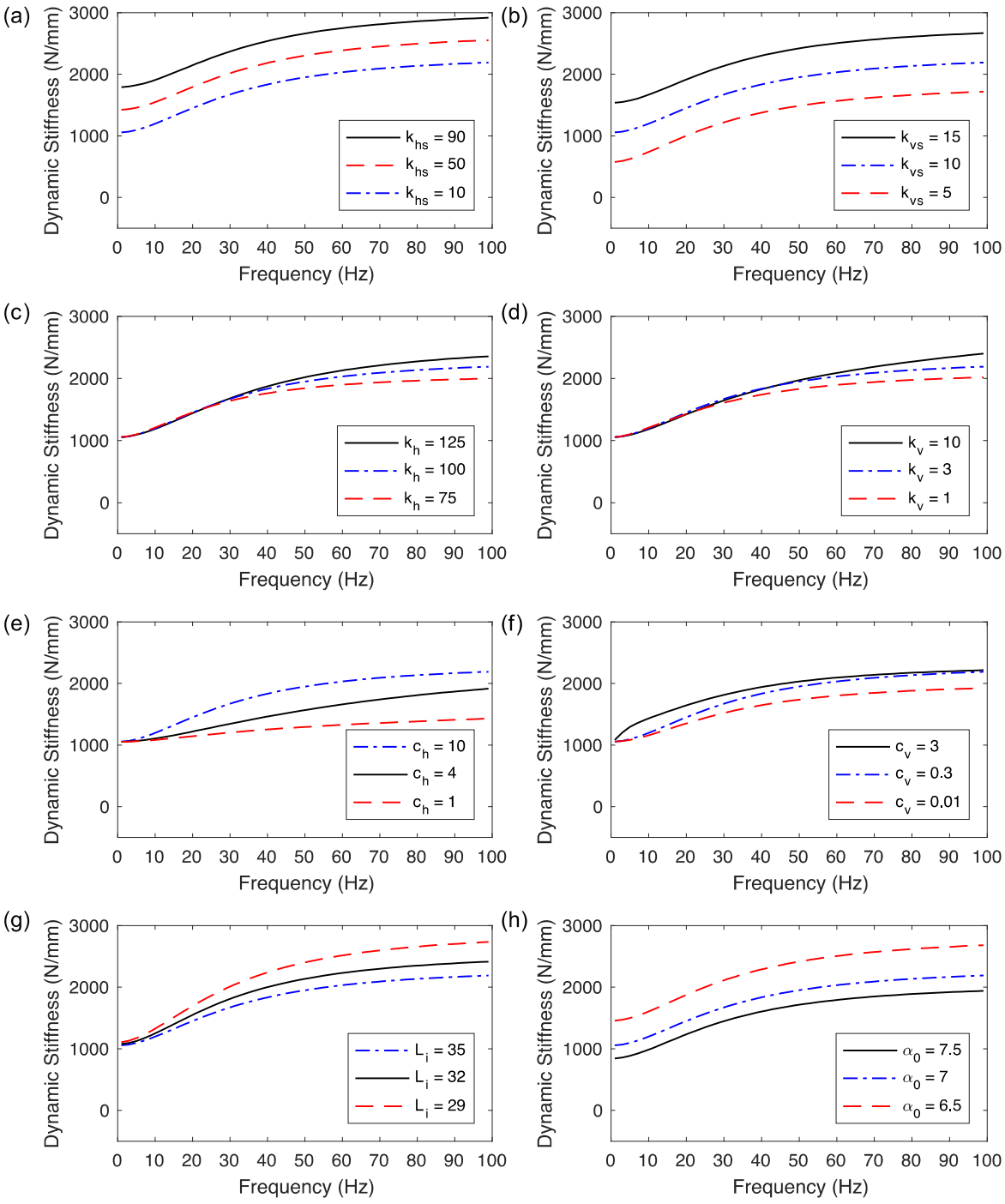

Fig. 8. The effects of (a) k_{hs}, (b) k_{vs}, (c) k_h, (d) k_v, (e) c_h, (f) c_v, (g) L_i, and (h) α_0 on the dynamic stiffness response of the mechanism under dynamic loading. k_h is taken as 100 N/mm, k_v is taken as 3 N/mm and c_v is taken as 0.3 Ns/mm for better comparison. Other values are from Table 1. The blue dashed-dotted line represents the response of the reference configuration.

is applied to the left joint in 0.05 s, then the mechanism is kept at that state for 10 s and the resistive force generated by the mechanism is calculated for different values of these parameters. As seen in Fig. 6a and b, k_{hs} and k_{vs} influence the steady state response of the system, while the amount of relaxation (the difference between the peak force and the steady-state force levels) and the relaxation rate remain the same. k_h and k_v mainly influence the start point of the relaxation curve (See Fig. 6c and d), whereas, c_h and c_v influence the relaxation rate (See Fig. 6e and f). L_i and α_0 affect the steady state response without altering the relaxation rate as seen in Fig. 6g and h.

Viscoelastic materials show different stress-strain responses during loading and unloading phases. The difference in force-displacement curves in loading and unloading phases gives rise to energy loss in each load cycle, which is called “hysteresis.” In order to observe the effects of the system parameters on the hysteresis response, the mechanism is compressively loaded and unloaded to 10 mm in 10 s. As seen in Fig. 7a and b, k_{hs} affects the stiffening part of the hysteresis curve, whereas k_{vs} affects the initial softening part and shifts the hysteresis curve. Similarly, k_h mainly affects the stiffening part of curve, while k_v affects mainly the softening part (See Fig. 7c and d). However, as the loading and unloading

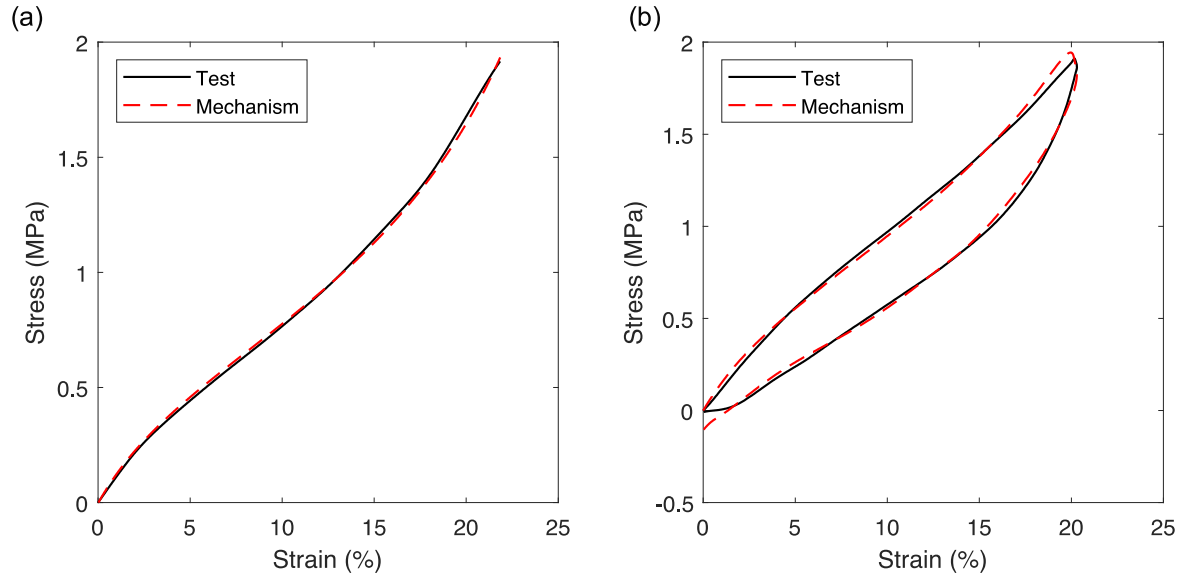

Fig. 9. Comparison of the mechanism response and the material response reported by Bergstrom and Boyce (2000) for (a) quasi-static loading and (b) hysteresis loading.

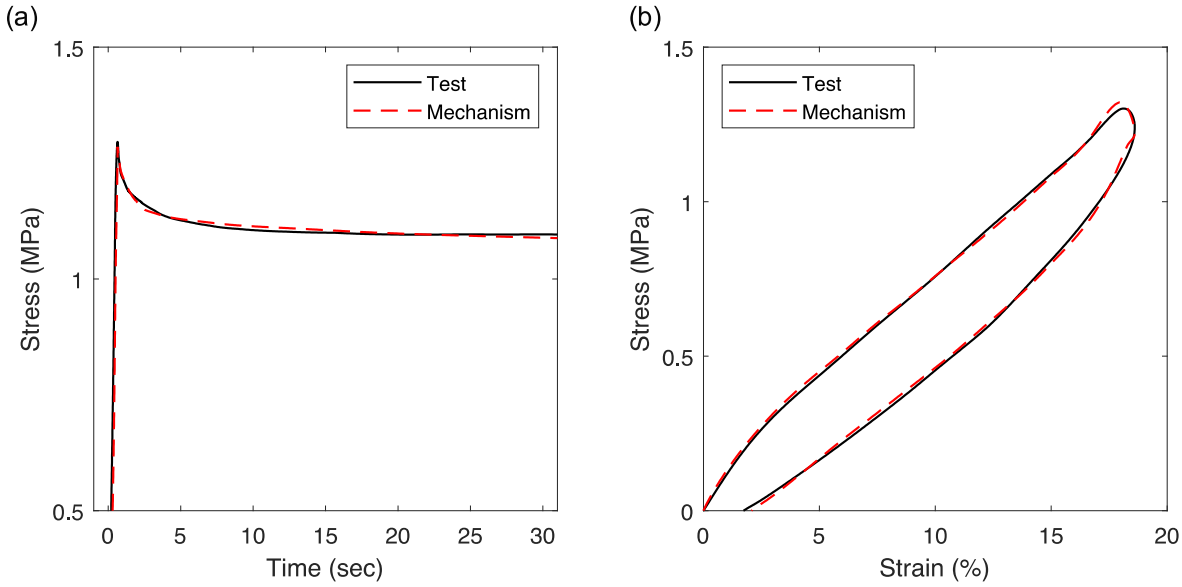

Fig. 10. Comparison of the mechanism response and the material response reported by Ciambella et al. (2010) for (a) ramp-and-hold loading and (b) hysteresis loading.

rates are low, the effect of k_{hs} and k_{vs} are more pronounced then k_h and k_v. On the other hand, k_h and k_v are more effective than k_{hs} and k_{vs} in changing the amount of hysteresis. As seen in Fig. 7e and f, c_h mainly affects the end of the loading cycle (stiffening part of the curve), whereas c_v affects mainly the end of the unloading cycle. Besides, both of these variables are effective in changing the amount of hysteresis. Decrease in L_i leads to a significant increase in the resistive force in the stiffening part without changing the low-displacement characteristics (See Fig. 7g). Notice that, for the smaller value of L_i (34 mm) the inner mechanism tends to close at large displacements which results in a highly nonlinear force-displacement response. Similar to L_i, α_0 also affects the stiffening part of the curve, but its effect is less pronounced (compare Fig. 7g and h). Furthermore, α_0 changes the initial softening part of the loading curve whereas L_i has no effect on this part.

In order to observe dynamic stiffness response of materials, samples are repeatedly compressed and/or extended to the same strain with continually increasing frequencies. Visco-hyperelastic materials show higher stiffness at higher excitation frequencies. Dashpot elements in the proposed mechanism model impart this property to the system. If the frequency is increased while keeping the amplitude the same, the velocity increases; accordingly, the resistance force generated by the dashpots increases and thus the overall stiffness increases. Consequently, the proposed mechanism shows increasing stiffness response with increasing frequency. In order to see the effects of the parameters on the dynamic stiffness behavior of the mechanism, it is repeatedly compressed by 1 mm, while increasing the frequency from 0 Hz to 100 Hz and the resistive force applied by the mechanism is used for calculating the dynamic stiffness values. Fig. 8 shows the effects of the system parameters on the dynamic response. For the results in Fig. 8, k_h is taken as 100 N/mm, k_v is taken as 3 N/mm and c_v is taken as 0.3 Ns/mm for better comparison. Other values are from Table 1. When k_{hs} and k_{vs} are increased, the overall response is shifted upwards without changing the stiffening characteristics (See Fig. 8a and b). As seen in the Fig. 8c and d, k_h and k_v change the slope

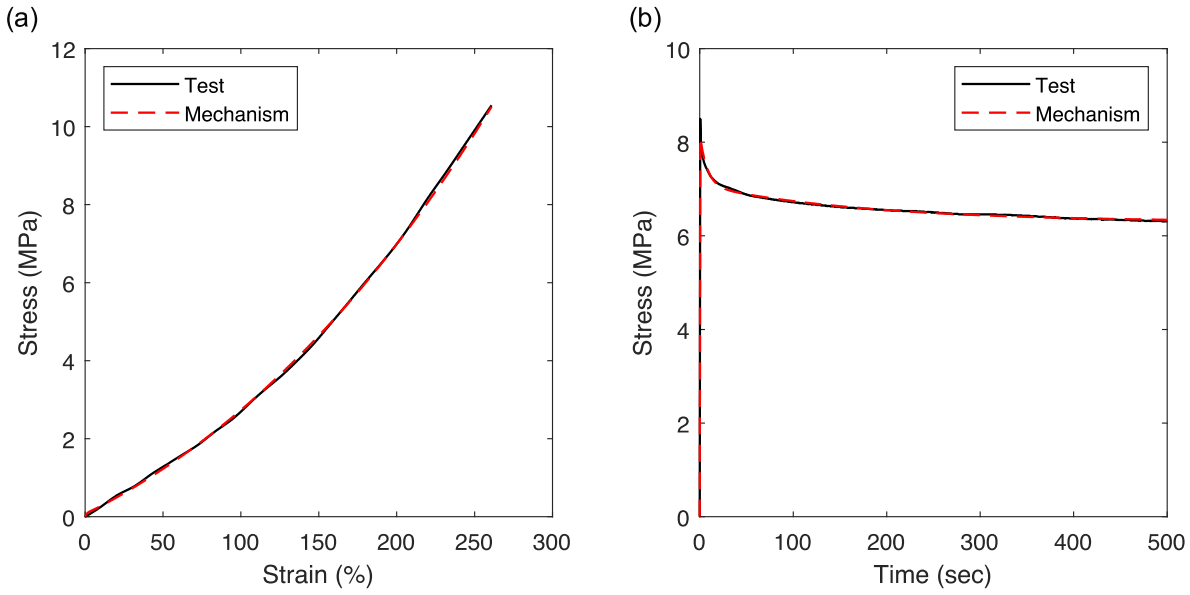

Fig. 11. Comparison of the mechanism response and the material response reported by Oman and Nagode (2014) for (a) quasi-static loading and (b) ramp-and-hold loading.

of the curve without changing the starting point. k_v is more dominant due to the dimensions of the system and the small amplitude excitation. c_h is effective on the slope of the response mainly in the intermediate and high frequencies without changing the initial point (See Fig. 8e). c_v is more effective at lower frequencies. As seen in Fig. 8f, larger values of c_v lead to increased stiffness of the mechanism at smaller frequencies as opposed to c_h. L_i shifts the dynamic stiffness response of the system at intermediate and high frequencies (See Fig. 8g). As it is seen in Fig. 8h, α_0 shifts the response without significantly altering stiffening characteristics.

4. Comparison of test data and model response

In order to see how well the mechanism simulates visco-hyperelastic material behavior, the response exhibited by the mechanism model is compared with the material response observed in experiments. As mentioned before, visco-hyperelastic material response in four test scenarios is simulated, which are quasi-static loading, ramp-and-hold loading, hysteresis loading, and dynamic loading. Unfortunately, no study in the literature simultaneously presents test data obtained under all these four different loading conditions for a visco-hyperelastic material. Comparisons are made with the studies that include two different loading conditions simultaneously.

In order to make comparisons, first, image-processing software (GetData) is used to generate data points from the curves given in previous studies. Then, the parameter values of the mechanism model are optimized so that its response fits the test data. For this purpose, objective functions are defined representing the difference between the measured material response and the calculated model response. Each data point of the model response is subtracted from the target data. These individual differences are used for calculating the total error by summing their squares. The sum of total errors of the two individual test scenarios are minimized for reducing the difference between the model response and the test results. The optimization problem formulation is given below

$$\min \; f = \sum_{i=1}^{n} (T_{1i} - R_{1i})^2 + \sum_{i=1}^{n} (T_{2i} - R_{2i})^2 \tag{28}$$

where R_{1i} and R_{2i} are the data points on the first and second response curves obtained from two different test scenarios and T_{1i} and T_{2i} are the data points of the corresponding target curves, respectively. Moreover, there are n data points on each curve. To solve the optimization problem, lower and upper limits of the parameters are defined. Random values are chosen between these limits to define the initial configuration of the mechanism as starting point of the optimization. Two curve fits among four different alternatives (quasi-static, ramp-and-hold, hysteresis, dynamic stiffness) will be satisfied with the same parameter values. Nonlinear-least square curve fit solver is used in MATLAB for the optimization process. Trust-region-reflective algorithm is used to minimize the objective function. In order to eliminate worse local minima, the optimization process in repeated 750 times starting from randomly chosen initial points. The strain values for the proposed mechanism in below figures are calculated as the ratio of applied displacement to initial horizontal length of the mechanism.

Bergstrom and Boyce, 2000 provided quasi-static and hysteresis loading test results for elastomers (chloroprene and natural rubber with carbon black). The strain rate was 0.01/s for compressive hysteresis loading. The material response is simulated by the mechanism model with the optimized parameter values of k_{hs} = 0.00779 N/mm, k_h = 0.0087 N/mm, c_h = 0.0008 Ns/mm, k_{vs} = 0.0048 N/mm, k_v = 13.1 N/mm, c_v = 0 Ns/mm, L_o = 100 mm, L_i = 35.1 mm, and α_o = 7.211° for both loading cases. As seen in Fig. 9, quasi-static response is closely approximated, while a small deviation appears in the hysteresis response at the end of the loading phase.

Ciambella et al., 2010 provided ramp-and-hold and hysteresis loading test results for a cylindrical carbon-black-filled rubber. The strain rate was 1.09/s for compressive hysteresis loading and the duration of the compression was 0.7 s for ramp-and-hold loading. The material response is simulated by the mechanism model with parameter values of k_{hs} = 0.01347 N/mm, k_h = 0.025 N/mm, c_h = 0.1199 Ns/mm, k_{vs} = 0.002688 N/mm, k_v = 0.002268 N/mm, c_v = 0.00054 Ns/mm, L_o = 100 mm, L_i = 34.73 mm, and α_o = 6.285°. As seen in Fig. 10, both ramp-and-hold loading and hysteresis loading scenarios are well simulated with the proposed model.

Oman and Nagode provided quasi-static and ramp-and-hold loading test results for filled rubber (Oman and Nagode, 2014). The main purpose of that study was to understand the material responses under different loading scenarios of creep and stress-relaxation tests. The material response is simulated by the present

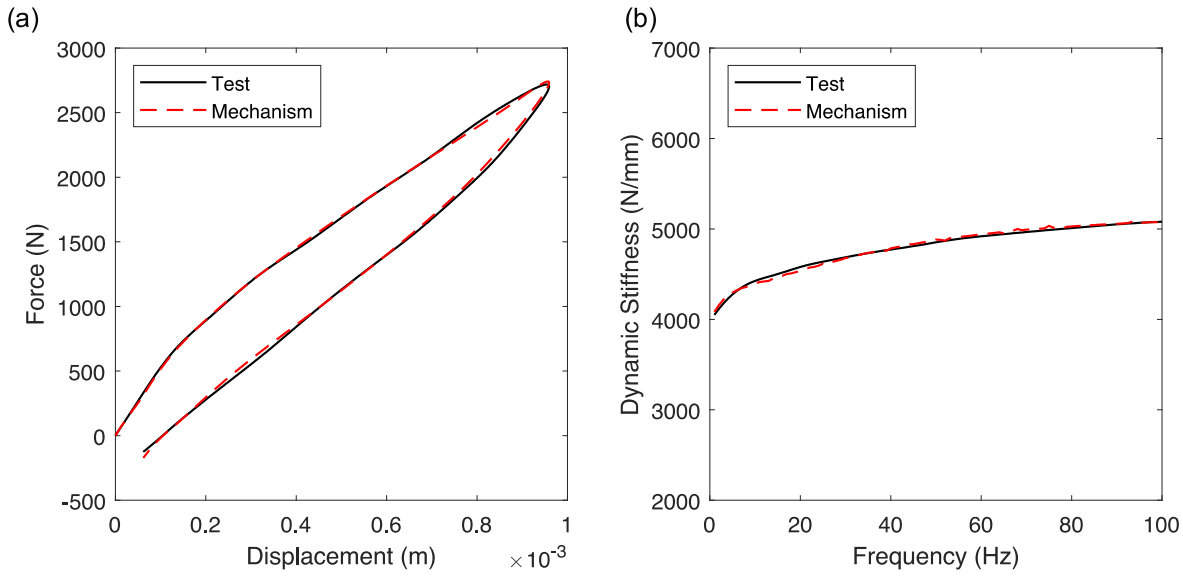

Fig. 12. Comparison of the mechanism response and the material response reported by Tarrago and Leif [Garcia Tarrago et al., 2007] for (a) hysteresis loading and (b) dynamic loading.

mechanism model with parameter values of $k_{hs} = 0.00248$ N/mm, $k_h = 0.04518$ N/mm, $c_h = 0.02036$ Ns/mm, $k_{vs} = 45.33$ N/mm, $k_v = 5.686$ N/mm, $c_v = 58.01$ Ns/mm, $L_o = 100$ mm, $L_i = 99.54$ mm, and $\alpha_o = 84.43°$ under tensile quasi-static loading and instantaneous tensile ramp-and-hold loading . As seen in Fig. 11, the mechanism mimics the material response obtained in quasi-static and ramp-and-hold tests quite well.

Tarrago and Leif (Garcia Tarrago et al., 2007) conducted a study on carbon-black filled rubber bushings to reveal the effects of amplitude and frequency on axial dynamic stiffness. The frequency of the compressive hysteresis load was 0.1 Hz and the range of frequency for dynamic loading was 0–100 Hz. The first loop of the hysteresis curves is used for comparison. The material response is simulated by the mechanism model with parameter values of $k_{hs} = 0.08245$ N/mm, $k_h = 21.42$ N/mm, $c_h = 26.2$ Ns/mm, $k_{vs} = 13.22$ N/mm, $k_v = 2.993$ N/mm, $c_v = 0.2359$ Ns/mm, $L_o = 100$ mm, $L_i = 34.93$ mm and $\alpha_o = 7.263°$. As seen in Fig. 12, the response of the mechanism model and the material response in hysteresis and dynamic stiffness tests compare very well.

5. Conclusions

A mechanism model is proposed to simulate the response of visco-hyperelastic materials under quasi-static, ramp-and-hold, hysteresis, and dynamic loading conditions. The geometric nonlinearity of the mechanism arising from the two nested four-bar linkages is used to mimic material nonlinearity. Various parametric studies are conducted to show the versatility of the proposed mechanism model in capturing the response under the aforementioned four different loading conditions. Comparisons with the experimental results obtained in previous studies show that the proposed mechanism model successfully represents nonlinear responses of visco-hyperelastic materials.

Since a visco-hyperelastic material was not tested in the previous studies by implementing all these four test scenarios on the same material, comparisons could only be made for the reported cases. As a future study, rubber-like materials will be selected and tested under these four loading conditions and the parameters of the mechanism model will be optimized to fit the data in order to show that the response of such a material under the four loading conditions can be simulated by the mechanism model using the same set of parameter values.

The mechanism model introduced in this study contains basic structural elements, i.e., links, linear springs, and dashpots. Hence, it can be physically realized. It can be used in various applications as a mechanical system behaving like a rubber. While exhibiting the mechanical response of rubber, the system would not have the undesired properties of rubber like thermal degradation or aging. Considering that individual parts are easily replaceable, the mechanism can be tuned to obtain the desired response.

Declaration of Competing Interests

The authors declare that they have no known competing financial interests or personal relationships that could have appeared to influence the work reported in this paper.

References

Abe, M., Yoshida, J., Fujino, Y., 2004. Multiaxial behaviors of laminated rubber bearings and their modeling. II: modeling. J. Struct. Eng. 130, 1133–1144. doi:10.1061/(ASCE)0733-9445(2004)130:8(1133).

Acar, G., Yilmaz, C., 2013. Experimental and numerical evidence for the existence of wide and deep phononic gaps induced by inertial amplification in two-dimensional solid structures. J. Sound. Vib. 332, 6389–6404. doi:10.1016/j.jsv.2013.06.022.

Agoras, M., Lopez-Pamies, O., Castaneda, P.P., 2009. A general hyperelastic model for incompressible fiber-reinforced elastomers. J. Mech. Phys. Solids 57, 268–286. doi:10.1016/j.jmps.2008.10.014.

Bergstrom J, S., Boyce M, C., 1998. Constitutive modeling of the large strain time-dependent behavior of elastomers. J. Mech. Phys. Solids 46, 931–954. doi:10.1016/s0022-5096(97)00075-6.

Bergstrom J, S., Boyce M, C., 2000. Large strain time-dependent behavior of filled elastomers. Mech. Mater. 32, 627–644. doi:10.1016/s0167-6636(00)00028-4.

Bhuiyan A, R., Okui, Y., Mitamura, H., Imai, T., 2009. A rheology model of high damping rubber bearings for seismic analysis: identification of nonlinear viscosity. Int. J. Solids Struct. 46, 1778–1792. doi:10.1016/j.ijsolstr.2009.01.005.

Buhan M, D., Gloria, A., Tallec P, L., Vidrascu, M., 2015. Reconstruction of a constitutive law for rubber from in silico experiments using Ogden's laws. Int. J. Solids Struct. 62, 158–173. doi:10.1016/j.ijsolstr.2015.02.026.

Carleo, F., Busfield, J.J.C., Whear, R., Barbieri, E., August 2017. A new constitutive model for carbon-black reinforced rubber in medium dynamic strains and medium strain rates. In: 10th European Conference on Constitutive Models for Rubber, ECCMR X 2017, Munich, Germany, pp. 28–31 115-119.

Ciambella, J., Paolone, A., Vidoli, S., 2010. A comparison of nonlinear integral-based viscoelastic models through compression tests on filled rubber. Mech. Mater. 42, 932–944. doi:10.1016/j.mechmat.2010.07.007.

Drozdov A, D., 1997. A constitutive model for nonlinear viscoelastic media. Int. J. Solids Struct. 34, 2685–2707. doi:10.1016/s0020-7683(96)00178-3.

Feng, B., Gan R, Z, October 2002. A lumped-parameter mechanical model of human ear for sound transmission. In: Proceedings of the Second Joint EMBS/BMES Conference, Houston, TX, USA, pp. 23–26 267-268.

Garcia Tarrago, M.J., Vinolas, J., Kari, L., 2007. Axial stiffness of carbon black filled rubber bushings frequency and amplitude dependence. Kautsch. Gummi Kunstst. 60, 43–48 oai:DIVA.org:kth-5875.

Hegde, S., Ananthasuresh G, K., 2012. A spring-mass-lever model, stiffness and inertia maps for single-input, single-output compliant mechanisms. Mech. Mach. Theory 58, 101–119. doi:10.1016/j.mechmachtheory.2012.01.006.

Holecek, M., Moravec, F., 2006. Hyperelastic model of a material which microstructure is formed by “balls and springs”. Int. J. Solids Struct. 43, 7393–7406. doi:10.1016/j.ijsolstr.2006.06.031.

Iniguez-Macedo, S., Lostado-Lorza, R., Escribano-Garcia, R., Martinez-Calvo, M.A, 2019. Finite element model updating combined with multi-response optimization for hyper-elastic materials characterization. Materials (Basel) 12 (7), 1019. doi:10.3390/ma12071019.

Kamaruddin, S., Chai, A.B., Lim, C.L., Ho, J.H., 2017. Characterization of static and dynamic response of natural rubber bio-composites. J. Phys. 908 (1), 012028. doi:10.1088/1742-6596/908/1/012028.

Khajehsaeid, H., Arghavani, J., Naghdabadi, R., 2013. A hyperelastic constitutive model for rubber-like materials. Eur. J. Mech. A/Solids 38, 144–151. doi:10.1016/j.euromechsol.2012.09.010.

Kim, K., Lee, J., Ju, J., Kim D, M., 2014. Compliant cellular materials with compliant porous structures: a mechanism based materials design. Int. J. Solids Struct. 51, 3889–3903. doi:10.1016/j.ijsolstr.2014.07.006.

Lewandowski, R., Chorazyczewski, B., 2010. Identification of the parameters of the Kelvin-Voigt and the Maxwell fractional models, used to modeling of viscoelastic dampers. Comput. Struct. 88, 1–17. doi:10.1016/j.compstruc.2009.09.001.

Mansouri M, R., Darijani, H., 2014. Constitutive modeling of isotropic hyperelastic materials in an exponential framework using a self-contained approach. Int. J. Solids Struct. 51, 4316–4326. doi:10.1016/j.ijsolstr.2014.08.018.

Muliana, A., Rajagopal K, R., Tscharnuter, D., Pinter, G., 2016. A nonlinear viscoelastic constitutive model for polymeric solids based on multiple natural configuration theory. Int. J. Solids Struct. 100–101, 95–110 10.1016 /j.ijsolstr.2016.07.017.

Natsupakpong, S., Cavusoglu, M.C., 2010. Determination of elasticity parameters in lumped element (mass-spring) models of deformable objects. Graph. Models 72, 61–73. doi:10.1016/j.gmod.2010.10.001.

Noborio H., Oohara T. On the repeatability of octree-based rheology mass-spring-damper model. International Workshop on Haptic Audio Visual Environments and Games, Lecco, Italy 7–8 November 2009;93-98

Oman, S., Nagode, M., 2014. Observation of the relation between uniaxial creep and stress relaxation of filled rubber. Mater. Des. 60, 451–457. doi:10.1016/j.matdes.2014.04.036.

Osterlof, R., Wentzel, H., Kari, L., Diercks, N., Wollscheid, D., 2014. Constitutive modeling of the amplitude and frequency dependency of filled elastomers utilizing a modified boundary surface model. Int. J. Solids Struct. 51, 3431–3438. doi:10.1016/j.ijsolstr.2014.06.003.

Pellicer, M., Morales J, S., 2004. Analysis of a viscoelastic spring-mass model. J. Math. Anal. Appl. 294, 687–698. doi:10.1016/j.jmaa.2004.03.008.

Ren, Y., Zhao, S., Yao, Q., Li, Q., Zhang, X., Zhang, L., 2015. Effects of plasticizers on the strain-induced crystallization and mechanical properties of natural rubber and synthetic polyisoprene. R. Soc. Chem. 5, 11317–11324. doi:10.1039/c4ra13504k.

Renaud, F., Dion J, L., Chevallier, G., Tawfiq, I., Lemaire, R., 2011. A new identification method of viscoelastic behavior: application to the generalized Maxwell model. Mech. Syst. Signal Process. 25, 991–1010. doi:10.1016/j.ymssp.2010.09.002.

Rendek, M., Lion, A., 2010. Amplitude dependence of filler-reinforced rubber: experiments, constitutive modeling and FEM-implementation. Int. J. Solids Struct. 47, 2918–2936. doi:10.1016/j.ijsolstr.2010.06.021.

Rey, T., Chagnon, G., Favier, D., Cam J B, L., 2014. Hyperelasticity with rate-independent microsphere hysteresis model for rubberlike materials. Comput. Mater. Sci. 90, 89–98. doi:10.1016/j.commatsci.2014.03.068.

San-Vicente, G., Aguinaga, I., Celigueta, J.T., 2012. Cubical mass spring model design based on a tensile deformation test and nonlinear material model. IEEE Trans. Vis. Comput. Graph. 18, 228–241. doi:10.1109/tvcg.2011.32.

Saitoh, M., 2012. A one dimensional lumped parameter model representing impedance functions in general structural systems with proportional damping. Int. J. Numer. Methods Eng. 90, 353–368. doi:10.1002/nme.3323.

Tam N, Q., Violaine, T., Christophe, F., 2015. The modeling of nonlinear rheological behavior and Mullin’s effect in high damping rubber. Int. J. Solids Struct. 75–76. doi:10.1016/j.ijsolstr.2015.08.017, 235-246.

Vandenbroucke, A., Laurent, H., Hocine N, A., Rio, G., 2010. A hyperelasto-visco-hysteresis model for an elastomeric behavior: experimental and numerical investigations. Comput. Mater. Sci. 48, 495–503. doi:10.1016/j.commatsci.2010.02.012.

Vieira A, C., Guedes, R.M., Tita, V., 2014. Constitutive modeling of biodegradable polymers: hydrolytic degradation and time-dependent behavior. Int. J. Solids Struct. 51, 1164–1174. doi:10.1016/j.ijsolstr.2013.12.010.

Wang, L., Han, Y., 2013. Compressive relaxation of the stress and resistance for carbon nanotube filled silicone rubber composite. Compos. Part A 47, 63–71. doi:10.1016/j.compositesa.2012.11.018.

Wollscheid, D., Lion, A., 2013. Predeformation – and frequency – dependent material behavior of filler - reinforced rubber: experiments, constitutive modeling and parameter identification. Int. J. Solids Struct. 50, 1217–1225. doi:10.1016/j.ijsolstr.2012.12.015.

Xu, X., Gao, S., Ou, Z., Ye, H, 2018. Mechanical behavior of liquid nitrile rubber-modified epoxy resin under static and dynamic loadings: experimental and constitutive analysis. Materials (Basel) 11 (9), 1565. doi:10.3390/ma11091565.

Yilmaz, C., Hulbert G, M., Kikuchi, N., 2007. Phononic band gaps induced by inertial amplification in periodic media. Phys. Rev. B 76, 054309. doi:10.1103/physrevb.76.054309.

Yilmaz, C., Hulbert G, M., 2010. Theory of phononic gaps induced by inertial amplification in finite structures. Phys. Lett. A 374, 3576–3584. doi:10.1016/j.physleta.2010.07.001.

Yuksel, O., Yilmaz, C., 2015. Shape optimization of phononic band gap structures incorporating inertial amplification mechanisms. J. Sound Vib. 355, 232–245. doi:10.1016/j.jsv.2015.06.016.

Zoffoli, L., Corti, E., Moro, D., Ponti, F., Ravaglioli, V, September 2017. Zero-dimensional model for dynamic behavior of engineered rubber in automotive applications. In: 72nd Conference of the Italian Thermal Machines Engineering Association, Lecce, Italy, pp. 6–8 939-946.